ORIGINAL ARTICLE

Magnetic tuned sorghum husk biosorbent for effective removal of cationic dyes from aqueous solution: isotherm, kinetics, thermodynamics and optimization studies

Abideen Idowu Adeogun[1] · James Asamu Akande[1] · Mopelola Abidemi Idowu[1] · Sarafadeen Olateju Kareem[2]

Abstract

Dyes containing effluents constitute hazards to the environments and endanger human and aquatic lives. Although activated charcoal has been adjudged the best for adsorption treatment of wastewater, its regeneration and high cost have limited their applications, hence the quest for alternative adsorbent. Magnetic tuned biosorbent was prepared from sorghum husks by in situ co-precipitation of Fe_3O_4. It was characterized using Fourier transform infrared spectroscopy, energy-dispersive X-ray spectroscopy and scanning electron microscopy. The biosorbent was then used for the removal of crystal violet (CV) and methylene blue (MB) dyes from aqueous solutions in a batch process. The effects of temperature, initial dye concentration, dosage, contact time as well as pH were investigated, and data obtained were analysed with appropriate kinetic and isotherm models. Response surface method was used for the optimization study of the adsorption using Box–Behnken experimental design. Pseudo-second-order kinetic model was the most appropriate model for both dyes with correlation coefficient $(R^2) > 0.9$ and low % standard error values. The equilibrium data were best fitted with Langmuir isotherm with maximum adsorption capacity (Q_{max}) of 18.87 and 30.00 mg g^{-1} for CV and MB, respectively. The thermodynamic parameters for the adsorption processes showed that it was spontaneous, endothermic and random systems with free energy changes less than zero, enthalpy changes (ΔH) of $+49.81$ and $+51.18$ kJ mol^{-1}, entropy changes (ΔS) of $+178.39$ and $+177.34$ J mol^{-1} K^{-1} for MB and CV dyes, respectively. Optimization studies revealed that 95% of the dyes are removable at 1.0 g adsorbent dosage and pH of 4.05 at 50 °C with initial dye concentration of 50 mg L^{-1}. The prepared adsorbent is cheap, easily recycled and highly effective for the treatment of dye-contaminated water.

Keywords Cationic dyes · Biosorption · Sorghum husk · Kinetics · Isotherm · Response surface

Introduction

Increased anthropogenic activities as a result of rapid urbanization and industrialization have led to the increase in environmental pollution with grave consequence in the quality of water available for industrial, agricultural and domestic use. Synthetic dyes and pigments are used extensively industrially and in many other fields of technology, leading to generation of highly coloured waste effluents (Hussein and Scholz

2018). These effluents are rich in dyes and chemicals, some of which are non-biodegradable and carcinogenic and pose a major threat to health and the environment. Furthermore, addition of synthetic dyes to water even at very low concentration (< 1 ppm) will impact negatively on the colour, which will inevitably affect the aesthetic merit, transparency as well as gas solubility of the water bodies. Reduced light penetration due to the presence of the coloured pollutants will result in the loss of photosynthesis and consequently upset the biological activities of the aquatic system which may lead to the destruction of aquatic species.

Methylene blue and crystal violet are cationic dye with various applications in chemistry, biology, medical science and dyeing industries, and they are highly toxic than other anionic dye (Gao et al. 2016). Methylene blue is widely used as hemp, silk fabric, stained paper dyeing, bamboo and wood colouring as well as a chemical agent in printing and dyeing enterprises

✉ Abideen Idowu Adeogun
  abuaisha2k3@yahoo.com

1 Chemistry Department, Federal University of Agriculture, Abeokuta, Abeokuta, Nigeria

2 Microbiology Department, Federal University ofAgriculture, Abeokuta, Abeokuta, Nigeria

(Ghosh and Bhattacharyya 2002); its adverse effects on human beings include: cyanosis, vomiting, diarrhoea, tachycardia and jaundice (Ait Ahsaine et al. 2018). Crystal violet is a triphenylmethane dye with poor degradability and carcinogenic inhaled or ingested (Saeed et al. 2010; Ahmad 2009); it is widely used in textile industries because of its low cost and high solubility in water (Ait Ahsaine et al. 2018). Medically, it is used as an antiseptic with a selective action on gram-positive organisms, also for the treatment of burns, boils, carbuncles and mycotic skin infections (Akinola and Umar 2015).

Dye effluents treatment may be a major task owing to the synthetic origins and aromatic structures of dyes which confers stability and made them to resist biologically degradation. Different methods including anaerobic/aerobic treatment, coagulation/flocculation, oxidation/ozonation, membrane separation and sorption had been applied to dye wastewater treatment. Of all these, adsorption process has proved to be outstanding technique from economical point of view, for colour removal from wastewater considering its initial cost, simplicity of design, ease of operation, insensitive to toxic substances and high removal efficiency (Ozdes et al. 2014; Pathania et al. 2010).

Activated carbon has been remarkably used for the treatment of dyes-contaminated wastewater due to their large surface area and porosity; however, regeneration and high cost have limited their applications. Agricultural by-products constitute environmental problems due to their availability in large quantity, especially after harvesting; also, their decomposition generates greenhouse gases that contribute to the global climate change. The utilization of agricultural waste as adsorbent in dye removal from wastewater is of great significance, and a number of agricultural waste materials had been studied for the removal of different dyes from aqueous solutions under different operating conditions (Bharathi and Ramesh 2013). Although the adsorbent from agricultural waste is cheap, the cost of regeneration, loss of adsorbent as well as reduction in adsorption capacity after regeneration are of great concern. In order to circumvent these problems, incorporation of magnetic particle into the adsorbent is hereby proposed; this is expected to produce a hybrid adsorbent with improved regeneration possibilities, significant adsorption capacity and economical feasibility.

This study therefore investigated the use of magnetic supported sorghum husk (MSH) for the effective removal of crystal violet and methylene blue dyes from aqueous solutions in a batch process. The effect of temperature, initial dye concentration, dosage, contact time and pH were investigated. The adsorption kinetic data were analysed using pseudo-first-order and pseudo-second-order kinetics, Elovich and intraparticle models. Equilibrium data were fitted to the Langmuir, Freundlich, Tempkin and Dubinin–Radushkevich isotherm models. Adsorption factors were optimized by Box–Behnken design.

Materials

Methylene blue and crystal violet which are chloride salts of 3,7-bis(dimethylamino)phenothiazin-5-ium and hexamethylpararosaniline (Fig. 1) with purity of 98% were obtained from Merck laboratory, India. Iron(III) chloride hexahydrate (99% $FeCl_3 \cdot 6H_2O$) and iron(II) chloride tetrahydrate (99% $FeCl_2 \cdot 4H_2O$) (AR grade) were products of Sigma-Aldrich. Hydrochloric acid and sodium hydroxide were procured from BDH, London. Other reagents were of analytical grade, and doubly distilled water was used for all of the experiments.

Preparation of the adsorbent

Sorghum husks (SHs) were obtained from a local farm at Odeda, Ogun State, Nigeria, the husks were washed under running tap to remove dirt and other impurities. The biomass was air-dried followed by oven-drying at temperature of 60 °C for 6 h. The dried biomass was pulverized and sieved to obtain powder with particle sizes less than 250 μm. The powder was then preserved in air-tight container until needed.

Magnetic modification of the adsorbent

A suspension containing 5.0 g of sorghum husk powder in 40 cm^3 of distilled water was prepared, and 20 cm^3 of 2 M urea solution was added into the mixture as stabilizer under continuous stirring. Solutions containing 20 cm^3 each of ferric chloride and ferrous chloride in ratio 2:1 molar concentration were added, the mixture was continuously stirred for 60 min, and then 20 ml of aqueous ammonia was added to adjust the pH to 11. The mixture was finally centrifuged, washed with deionized water and dried at 105 °C in a vacuum oven.

Characterization

The modified and unmodified adsorbents used after adsorption of dyes were characterized with Fourier transform infrared (FTIR) spectroscopy spectrophotometer (Bruker Tensor 27) in KBr pellets spectra in a range from 4000 to 400 cm^{-1}. Surface morphology and elemental composition of the magnetic
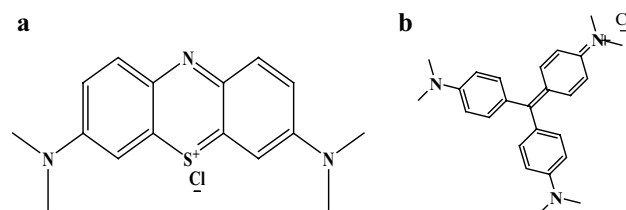

Fig. 1 Structures of the cationic dyes: **a** methyl blue and **b** crystal violet

biosorbent were analysed using scanning electron microscopy (SEM) [VEGA3 TESCAN] equipped with EDAX.

Preparations of aqueous solution of the dye

Stock solution of the dyes was prepared by dissolving accurately weighed solute (Fig. 1) such that the solution contained 1 g equivalent of the dyes in 1 dm^3 distilled water, and working standard solutions were then prepared from these stocks by dilution. The pH of the working solutions was adjusted with aliquot of HCl or NaOH prior to the adsorption study.

Adsorption studies

The batch equilibrium and kinetics adsorption studies were conducted in process in Erlenmeyer flasks containing 25 cm^3 of dye solutions with concentration range between 50 and 200 mg dm^{-3} and 0.1 g of the adsorbents. The contents were placed in a regulated water bath (30 ± 1 °C) with shaker at 150 rpm, and samples were collected at pre-set time intervals. The dye concentrations in aqueous media were determined after the adsorbent was removed magnetically, by reading the absorbance at 665 and 586 nm for MB and CV, respectively. The amount of dye adsorbed (mg g^{-1}) by the adsorbents as a function of time (Q_t) and at equilibrium (Q_e) was estimated according to Eqs. 1 and 2 below:

$$Q_t = \frac{(C_o - C_t)}{m} \times V \tag{1}$$

$$Q_e = \frac{(C_o - C_e)}{m} \times V \tag{2}$$

where C_o, C_t and C_e are the initial concentration, concentration at time t and equilibrium concentration (mg dm^{-3}) of the dye, respectively, V is volume (dm^{-3}) of the solution, and m is the mass (g) of the adsorbent.

Adsorption kinetics and isotherms studies

The kinetics of adsorption of the dyes onto the adsorbent were investigated by subjecting the data from time-dependent adsorption to pseudo-first-order (Ho and McKay 1999) and pseudo-second-order kinetics (Ho and McKay 1998), Elovich kinetics (Elovich and Larionov 1962) and intraparticle diffusion (Weber and Morris 1963) models to describe the mechanism of the adsorption process. The mathematical expressions of these models (Eqs. 3–6) are presented in Table 1. All data were analysed with nonlinear regression analysis method using a program written on MicroMath Scientist software (Salt Lake City, Utah, USA). Three error functions (Eqs. 7–9), the sum square error function (SSE), root mean square error (RMSE) and composite fractional error (HYBRD) were applied to confirm the kinetic models fitting (where N is the number of data and P is the number of parameters) along with the regression coefficient R^2. The lower the values of SSE, RMSE and HYBRD errors and the higher the value of R^2, the better the fitting of the model (Hanbali et al. 2014).

$$\text{SSE} = \sum_{i=1}^{N} (Q_{(\exp)} - Q_{(\text{cal})})^2 \tag{7}$$

$$\text{RMSE} = \sqrt{\frac{1}{N-2} \sum_{i}^{N} (Q_{(\exp)} - Q_{(\text{cal})})^2} \tag{8}$$

$$\text{HYBRD} = \frac{100}{N-P} \sqrt{\sum_{i=1}^{N} \left(\frac{(Q_{(\exp)} - Q_{(\text{cal})})}{Q_{(\exp)}} \right)^2} \tag{9}$$

Adsorption equilibrium data were also subjected to the Langmuir (1916), Freundlich (1906), Tempkin and Pyzhev (1940) and Dubinin and Radushkevich (1947) isotherm models (represented by Eqs. 10–13). The isotherm parameters were

Table 1 Kinetic model for the adsorption studies of CV and MB

Name	Model
Pseudo-first order	$Q_t = Q_e(1 - e^{-k_1 t})$ (3) where Q_e and Q_t are the amounts (mg g^{-1}) of dye adsorbed per unit mass of adsorbent at equilibrium time and time t, respectively, while k_1 (min^{-1}) is the rate constant for the pseudo-first-order kinetics
Pseudo-second order	$Q_t = \frac{k_2 Q_e^2 t}{1 + k_2 Q_e t}$ (4) where Q_e and Q_t are the amounts (mg) of dye adsorbed per unit mass of adsorbent at equilibrium time and time t, respectively, while k_2 (g mg^{-1} min^{-1}) is the rate constant for the pseudo-second-order kinetics
Elovich	$Q_t = {}^1/_\beta \ln(\alpha \beta * t)$ (5) where α (mg g^{-1}) is the initial adsorption rate constant and the parameter β (g mg^{-1} min^{-1}) is related to the extent of surface coverage and activation energy for chemisorptions
Intraparticle diffusion	$Q_t = K_{id} t^{0.5} + Ci$ (6) where K_{id} is the intraparticle diffusion rate constant (mg mg^{-1} min$^{-0.5}$) and C is a constant (mg mg^{-1}) which gives information about the thickness of boundary layer

obtained by the least square fit method as earlier mentioned. The mathematical expressions of these isotherm models (Eqs. 10–13) are presented in Table 2.

Thermodynamic parameters

The thermodynamic parameters, $\Delta G°$, $\Delta H°$ and $\Delta S°$, explain the feasibility, spontaneity and the nature of adsorbate–adsorbent interactions during the adsorption process (Adeogun et al. 2016). Their values were obtained from the temperature-dependent equilibrium study by viewing the process at equilibrium using the notation below:

$$A + B \rightleftharpoons A * B$$

The equilibrium constants in terms of the adsorbate (C_e), adsorbent dosage (m) and adsorbed quantity (Q_e) could be written as:

$$K_D = \frac{Q_e}{C_e * m} \tag{14}$$

$$\Delta G° = -RT \ln K_D \tag{15}$$

$$\Delta G° = \Delta H° - T\Delta S° \tag{16}$$

$$\ln K_D = \frac{\Delta S°}{R} - \frac{\Delta H°}{RT} \tag{17}$$

The van't Hoff plot (ln K_D vs. $1/T$) for the adsorption process gives the slope and intercept from which thermodynamic parameters were obtained.

Design of experiments

Experimental design of the adsorption process was achieved by response surface methodology (RSM). The Box–Behnken was selected for the optimization of the parameters

investigated for the adsorption of dyes; these include pH, dye initial concentration, adsorbent dosage and temperature. The adequacy of the employed model was ascertained using analysis of variance (ANOVA), while 3-D graphical analysis of the data was used to explain the interactions between the process variables and the response. The actual design was obtained using statistical software, Design-Expert V6.0.8 (Stat-Ease Inc., USA), with the factor set as shown in Table 3.

Results and discussion

Characterization of the adsorbent

SEM images of SH and MSH before and after adsorption are presented in Fig. 2a–c. Figure 2a reveals porous structure with large particle sizes characteristics of cellulosic materials. Figure 2b reveals a denser surface as a result of modification with iron oxide nanoparticles. The electrostatic interaction between the negatively charged oxygen atom of the cellulose hydroxyl groups of the cellulose and the positively charged Fe atom in the metal oxide along with condensation and hydrolysis reactions that accompany the addition of NH_4OH results in the incorporation of the magnetic particles into the bulk of the cellulose (Luo et al. 2010). After adsorption, the surface of the particle collapsed with a reduced pore

Table 3 Process factors and levels

Factors	Low (−1)	Mean (0)	High (+)
(x_1)—pH	2	6.5	11
(x_2)—Conc. (mg L^{-1})	10	30	50
(x_3)—Dosage (g)	0.05	0.525	1.00
(x_4)—Temp. (°C)	30	40	50

Table 2 Isotherm models applied for the adsorption of studies of CV and MB

| Name	Model
Langmuir	$Q_{eq} = \frac{Q_{max}bC_e}{1+bC_e}$ (10) where Q_{eq} and Q_{max} are the amounts (mg g^{-1}) of dye adsorbed per unit mass of adsorbent and maximum adsorption capacity at equilibrium, respectively, C_e is the equilibrium concentration of adsorbate, while b (L mg^{-1}) Langmuir constant
Freundlich	$Q_{eq} = K_F C_e^{1/n}$ (11) where K_F (mg g^{-1}) (L mg^{-1})$^{1/n}$ is a rough estimation of adsorption capacity of the adsorbent, $1/n$ is the adsorption intensity
Tempkin	$Q_e = \frac{RT}{b_T} \ln a_T C_e$ (12) R (J mol K^{-1}) is the gas constant, T (K) is absolute temperature, a_T (mg L^{-1}) is the binding constant, and b_T (L g^{-1}) is related to the heat of adsorption
Dubinin–Radushkevich	$Q_e = Q_s e^{-\beta \varepsilon^2}$ (13) where Q_s (mg g^{-1}) is the saturation capacity, β (mol J)^2 is a constant relation to adsorption energy, while ε is related to the mean free energy of adsorption and given $\varepsilon = RT * \ln\left(1 + \frac{1}{C_e}\right)$
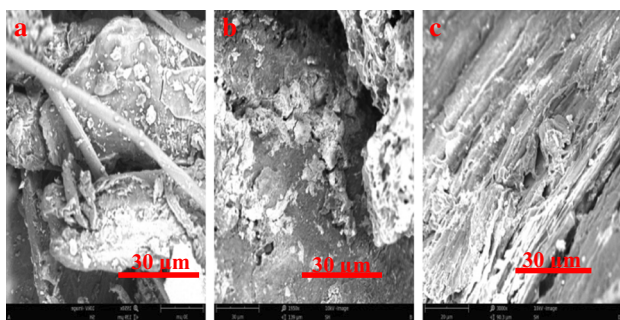
Fig. 2 SEM image of: **a** SH, **b** MSH and **c** MSH after adsorption of dyes

Fig. 4 FTIR spectra of (a) SH, (b) MSH and (c) MSH after adsorption of MB and (d) after adsorption of CV

size (Fig. 2c). The result of energy-dispersive X-ray (EDX) analysis further confirmed the incorporation of the magnetic particles, Fig. 3a shows that the sorghum husk is rich in carbon and oxygen, however, Fig. 3b, c shows the presence of Fe on the surface of the modified sample, and, however, Fig. 3c displays a reduced intensity possibly because of the adsorbed dye molecules interactions with adsorbent sites.

The FTIR spectra of adsorbent before and after adsorption are shown in Fig. 4. The broad bands around 3420 cm^{-1} in the spectra of the SH were slightly shifted to 3470 cm^{-1} in the MSH, and these peak were assigned to the intramolecular hydrogen bond due to the O–H group in the adsorbent. The peaks around 1700 cm^{-1} correspond to the C=O stretch. The absorption peak around 600 cm^{-1} noted in the MSH could be attributed to the characteristic absorption peak of Fe$_3$O$_4$ (Schwertmann and Cornell 2008; Pereira and Alves 2012) indicating the stability of the magnetic components within the SH matrix. The effect of modification and adsorption is outlined in the circled
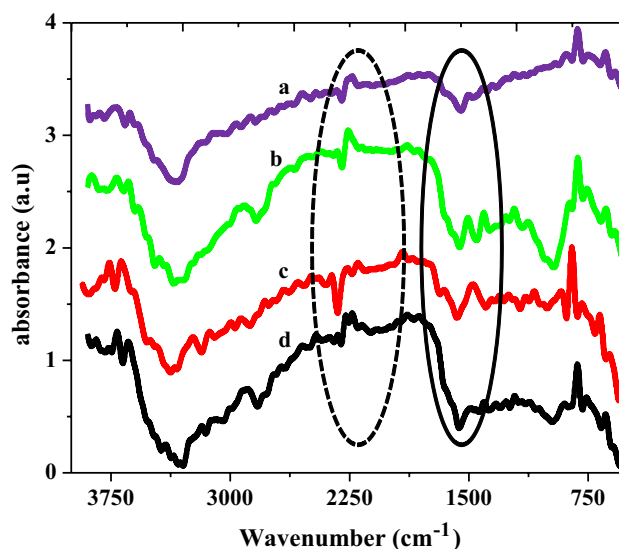
area in the FTIR spectra, and the continuos circle displays the modification with Fe–O at around 510 cm^{-1} which is conspicuously missing in the raw sample, while the areas demarcated with dashed circle show the difference in adsorption of the dyes onto the adsorbent.

Effect of contact time

The removal of the dyes from aqueous solution depends on the initial dye concentration and contact time as shown in Fig. 5. The quantities of dyes removed increase with initial concentration and the progress of the adsorption with time,
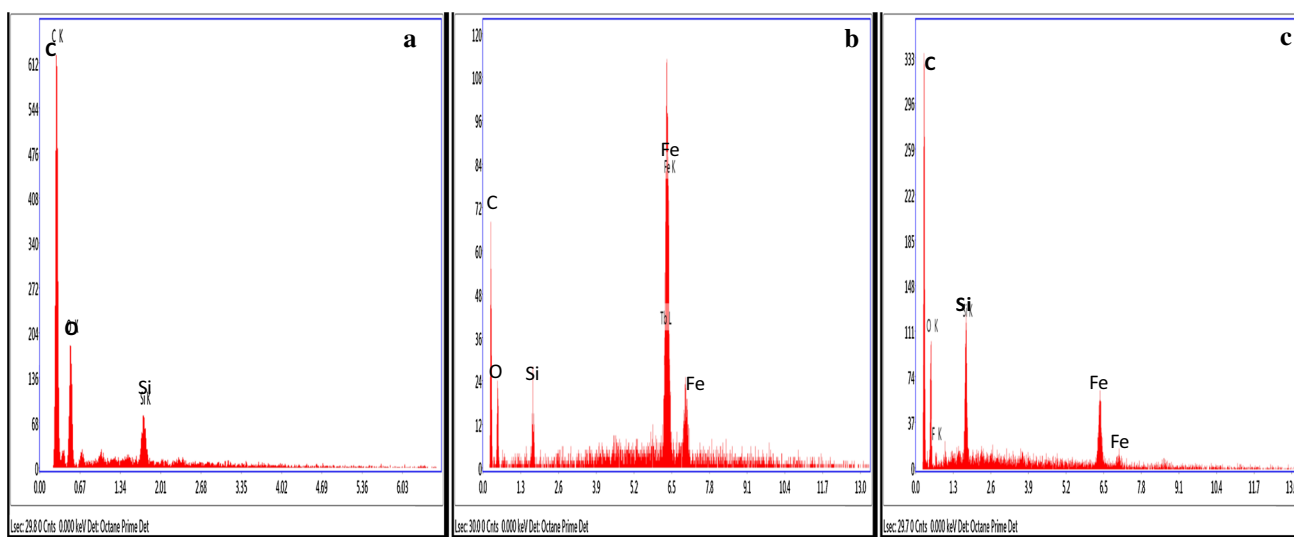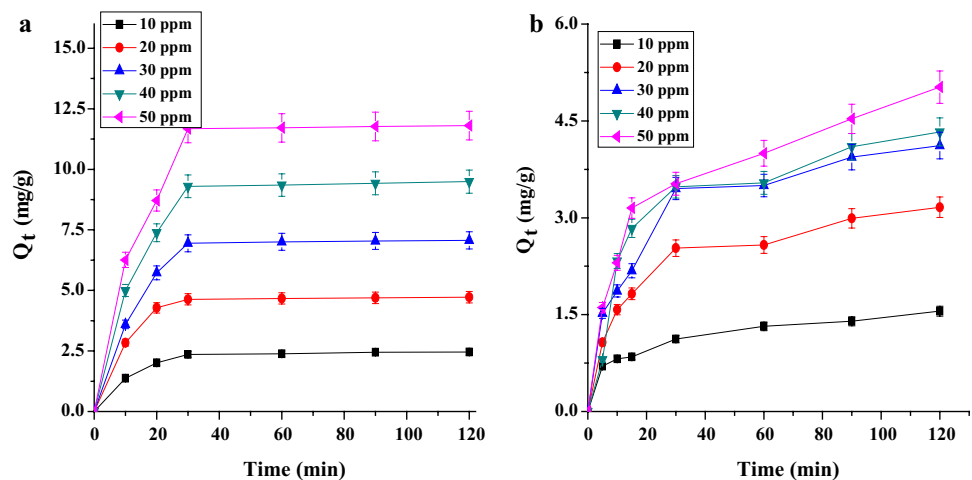

Fig. 3 EDX analysis of **a** SH, **b** MSH and **c** MSH after adsorption

and there was a rapid removal of MB (Fig. 5a) in the first 10 min and this was maintained for the next 20 min before the process continued steadily. Similarly, the removal of CV (Fig. 5b) progresses quickly for the first 20 min and this was sustained till equilibrium was established. Adsorption capacities at equilibrium increase from 2.45 to 11.81 mg g^{-1} for MB, while those of CV increase from 2.41 to 8.16 mg g^{-1} as their initial concentrations increase from 10 to 50 ppm.

Influence of pH on the removal of CV and MB by MSH

The influence of pH of the media on the adsorption process cannot be over-emphasized, especially dye removal. It affects the chemical properties of the dye solution, and also the surface charge of the adsorbent as well as interactions in the media depends on the pH (Ait Ahsaine et al. 2018). The removal efficiency of both dyes increases as the pH of the media increases as shown in Fig. 6. The maximum removal

efficiency of about 97% was obtained for the MB at pH 9, while that of CV was 95% at pH 8. At lower pH, the presence of H$^+$, a cation which competes with dye molecules for the available adsorption sites, resulted in lower adsorption; however, as the pH increases, the competition for the available site reduces, while the interaction between the adsorbent and dye molecules increases leading to an increase in removal efficiency (Bestani et al. 2008).

Adsorbent dosage studies

The effect of adsorbent dosage on the removal efficiency of CV and MB by MSH is shown in Fig. 7. As the adsorbent dosage increases from 0.05 to 0.4 g, the removal efficiency increases from observed that as the quantity of the adsorbent increased from 0.05 to 0.6 g, the removal efficiency increased from 95.9 to 98.6% for MB; on the other hand, that of CV increases from 96.4 to 98.4%. These increased efficiencies may be attributed to the increase in adsorption
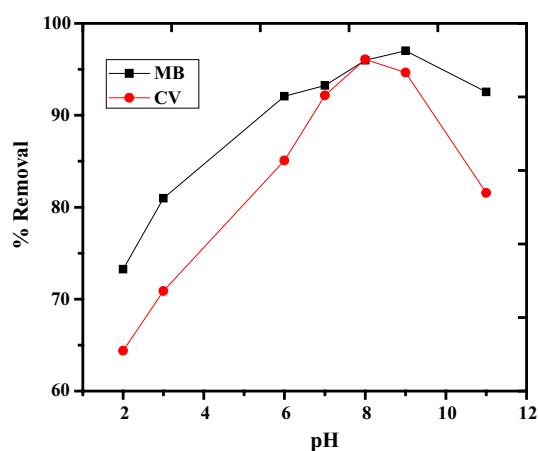

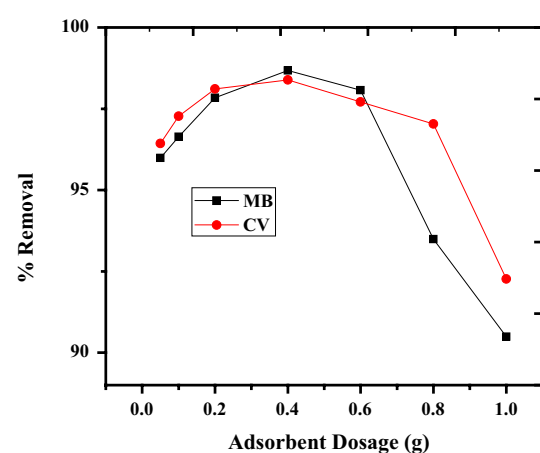**Fig. 6** The influence of pH on the removal efficiency of CV and MB by MSH

Fig. 7 The influence of adsorbent dosage on the removal efficiency CV and MB by MSH

sites as the dosage increases, and the decrease in efficiencies noted with further increase in the adsorbent dosage resulted from particle interactions, including percolation which collapsed the active sites on the adsorbent (Raveendra et al. 2014; Kakavandi et al. 2016).

Effect of temperature

The effects of temperature on the removal efficiency of CV and MB were investigated between 30 and 50 °C. Figure 8 shows that adsorption capacities increase with increase in temperature due to increase in contact rates of dye molecules with the adsorbent as well as increase in diffusion rate into the pores of the adsorbent whose dimension also becomes enlarged with increased temperature leading to interaction of the dye molecules with the functional group within the adsorbent (Wong et al. 2007).

Adsorption kinetics

The understanding of the mechanism of adsorption is a function of elaborate analysis of the time-dependent adsorption data. The adsorption process is characterized by mechanisms such as chemical interactions between the adsorbent and adsorbate, diffusion or mass transfer of the adsorbate into and within the adsorbent or combination of these mechanisms, and hence, combinations of models are required to elucidate the mechanism of adsorption. The pseudo-first-order and pseudo-second-order kinetics as well as intraparticle diffusion and Elovich models were used to examine the kinetic of adsorption of MB and CV by MSH. The model fits for the MB and CV adsorption are shown in Figs. 8 and 9, while the parameters for these fits are presented in Tables 4 and 5.

The parameters of pseudo-first-order and pseudo-second-order kinetics models presented in Table 4 and Figs. 9a, b and 10a, b showed that the models fitted the adsorption of
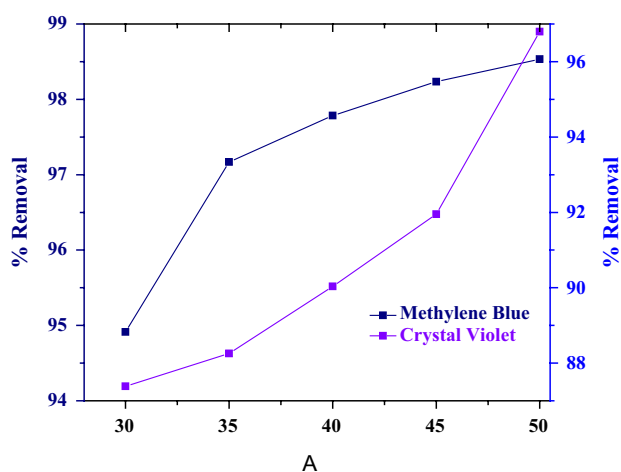

Fig. 8 Effect of temperature on the removal of CV and MB by MSH

MB and CV by MSH. The value of the regression coefficients R^2 for the models is > 0.99; however, taking the cognizance of the error function analyses and the closeness of the Q_e determined experimentally with the theoretical values showed that the first-order kinetic model is much favoured, suggesting physical interactions between adsorbent and adsorbate. Similarly, the Elovich model fit (Figs. 9c, 10c) agreed with the experimental data, the parameters (Table 5), showed that $R^2 > 0.99$, the values β_{el} showed that the available site for adsorption decreases with increase in dye concentrations with increasing concentration of adsorbed quantity, α_{el}. The positive values of these constants confirmed the sorption, and hence, Elovich model properly explained the initial kinetics of adsorption of the dyes onto the adsorbent as previously reported in the literature (Vassileva et al. 2013; Cheu et al. 2016). The intraparticle diffusion model suggested multilinearity adsorptions, the two dyes adsorbed in a biphasic process as depicted in Figs. 8d and 9d, and the parameters (Table 5) showed that these phases are of nonzero intercept. These indicate that intraparticle diffusion is not the only rate-controlling step and that external mass transfer also has played an important role in the transfer of the dyes into the adsorbent (Maksin et al. 2012; Rathod et al. 2014).

Adsorption isotherms models

Proper understanding of adsorption process basically depends on information obtainable from equilibrium adsorption. Interpretations of this information are critical to the overall improvement of adsorption mechanism pathways and effective design of adsorption system (El-Khaiary 2008). The adsorption isotherm model fits used to investigate the adsorption of MB and CV onto MSH are presented in Fig. 11a and b, and the parameters are shown in Table 6.

The isotherm parameters revealed that the entire isotherm model investigated here fits the data very well with R^2 in the order of Langmuir > Freundlich > Dubinin–Radushkevich > Tempkin for MB, while the order is Langmuir = Tempkin > Freundlich > Dubinin–Radushkevich for CV. This suggested a monolayer adsorption of the dyes onto the adsorbent with maximum adsorption capacities of 30.04 and 18.78 mg g^{-1} for MB and CV, respectively. The R_L values < 1 indicate a favourable adsorption. Freundlich parameters indicate the heterogeneity nature of the surface of adsorbent, and the $1/n$ values of < 1 indicate a normal Langmuir isotherm, otherwise cooperative adsorption (El-Sayed 2011). The Tempkin isotherm parameters and the R^2 values showed favourable fits for the dyes, and this implies that adsorption process is characterized by uniform distribution of binding energies. These isotherms do not described the saturation behaviour, hence the investigation with Dubinin–Radushkevich. From the table, the saturation
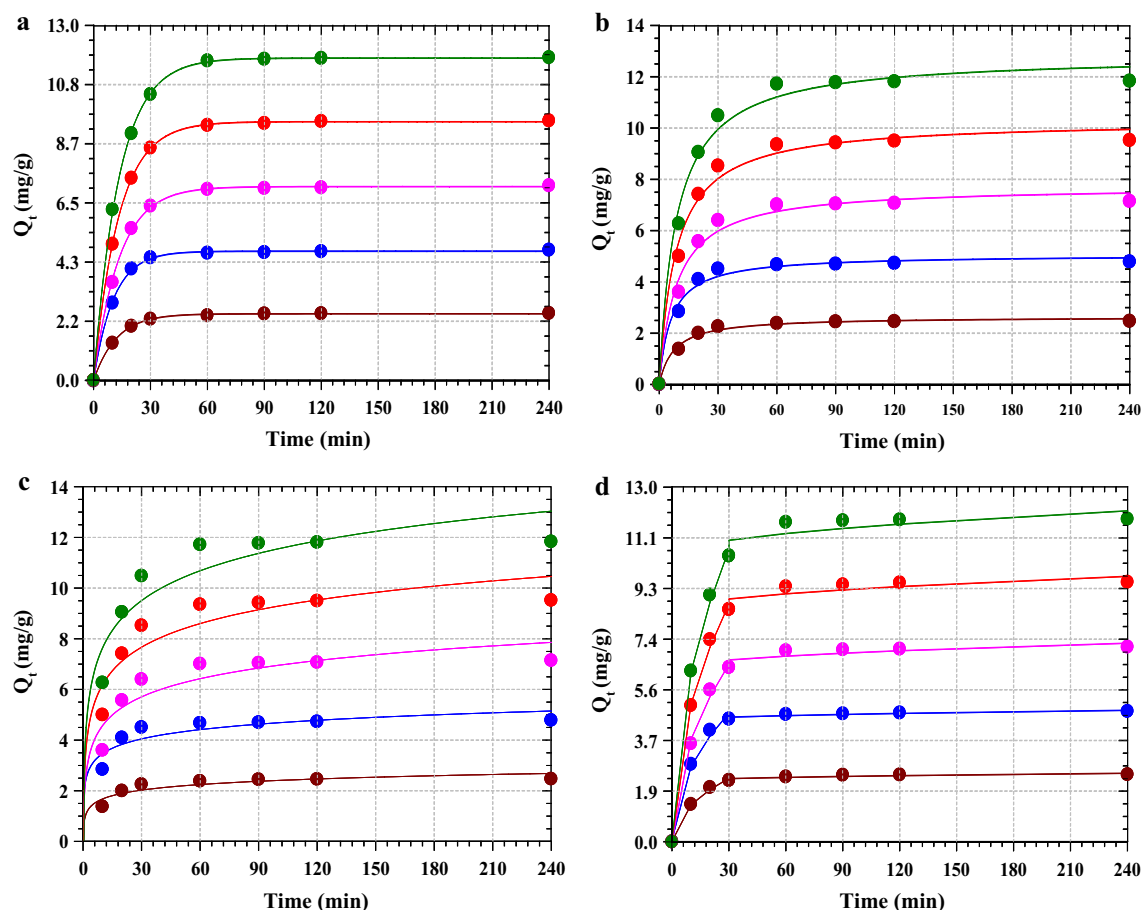
Fig. 9 Kinetics models fits of MB onto MSH: **a** pseudo-first order, **b** pseudo-second order, **c** Elovich and **d** intraparticle diffusion

capacities of the dyes are 21.13 and 15.33 mg g^{-1} for MB and CV, respectively. The mean free energies obtained for the adsorption of the dyes are < 8 kJ mol^{-1}, confirming the physisorption adsorption as suggested by the kinetic fit. Table 7 presents the comparison of the adsorption capacity of other adsorbents for the removal of MB and CV dyes. It is glaring from this table that MSH is compared favourably with other adsorbents in the same category for adsorption of MB and CV.

Adsorption statistical optimization studies

The interactions and significance of the independent variables were tested statistically by optimization studies using the experimental data, based on the Box–Behnken matrix in Table 8. The experimental results were used to optimize the process, and the combined effects of two parameters on the dyes removal efficiency were represented by the response surface and contour plots using Design-Expert 6.0 software (Stat-Ease Inc. Minneapolis, USA).

The significance of the model including the terms in the equation was determined from the analysis of variance

(ANOVA) using parameters such as the F-test, p value and the sum of squares, and the results are presented in Table 9. The higher F-values obtained for the dyes show that models are significant with p-values of < 0.0001 indicating that the contribution of the obtained values is insignificant. For the removal of the CV, adsorbent dosage was found to be more significant, while temperature is the most significant for the removal of MB among all the parameters given their highest sum of a square and F-test values, respectively (Dhawane et al. 2016). However, the combined effect of pH and adsorbent dosage on removal efficiency was dominant among all the possible combinations for both dyes, whereas dye concentration was the most dominants of the squared term. The non-significance obtained from the lack of fit value implied the perfect fit of experimental data in the chosen quadratic model. The correlation coefficients were estimated for the accuracy of experimental results as shown in Table 10, and the predicted R^2 and adjusted R^2 were in reasonable agreement with each other which implied that the variation of the mean and capability of the model to predict the response was in the acceptable range. Adequate precision measures the signal-to-noise ratio and

Table 4 Kinetic parameters for the adsorption of MB and CV onto MSH

	Methylene blue					Crystal violet				
The pseudo-first-order kinetics model parameters										
C_o (mg dm^{-3})	10	20	30	40	50	10	20	30	40	50
$Q_{e\,exp}$ (mg g^{-1})	2.465	4.781	7.141	9.515	11.83	1.817	3.695	4.746	4.705	5.009
$Q_{e\,cal}$ (mg g^{-1})	2.443	4.734	7.102	9.479	11.808	1.814	3.694	4.775	4.722	4.919
k_1 (min^{-1})	0.083	0.095	0.074	0.076	0.074	0.046	0.047	0.045	0.058	0.066
R^2	0.999	0.999	0.999	0.999	0.999	0.999	0.999	0.999	0.999	0.999
%SSE	0.008	0.009	0.003	0.001	0.000	0.000	0.000	0.004	0.001	0.032
RMSE	0.003	0.006	0.005	0.005	0.003	0.000	0.000	0.004	0.002	0.011
HYBRD	0.113	0.122	0.069	0.047	0.023	0.023	0.003	0.076	0.045	0.225
The pseudo-second-order kinetics model parameter										
$Q_{e\,cal}$ (mg g^{-1})	2.635	5.056	7.729	10.292	12.83	2.193	4.463	5.825	5.540	5.684
k_2 (g mg^{-1} min^{-1})	0.051	0.033	0.015	0.011	0.009	0.022	0.011	0.008	0.012	0.014
R^2	0.998	0.998	0.998	0.998	0.998	0.999	0.998	0.998	0.998	0.999
%SSE	0.476	0.331	0.678	0.667	0.714	4.288	4.310	5.175	3.147	1.815
RMSE	0.021	0.034	0.073	0.097	0.125	0.047	0.096	0.135	0.104	0.084
HYBRD	0.862	0.72	1.029	1.021	1.056	2.588	2.595	2.843	2.217	1.684
Elovich model's parameter										
$Q_{e\,cal}$ (mg g^{-1})	2.463	4.778	7.138	9.53	11.858	1.918	3.925	5.045	5.111	5.346
α_{el} (mg g^{-1} min^{-1})	6.3	7.103	8.613	13.415	15.326	0.228	0.465	0.559	0.764	0.990
β_{el} (g mg^{-1})	3.157	1.892	0.968	0.744	0.589	2.118	1.033	0.786	0.853	0.867
R^2	0.993	0.993	0.993	0.993	0.993	0.997	0.997	0.997	0.997	0.997
%SSE	0.000	0.000	0.000	0.000	0.000	0.003	0.004	0.004	0.007	0.005
RMSE	0.000	0.000	0.000	0.002	0.004	0.013	0.029	0.037	0.051	0.042
HYBRD	0.008	0.006	0.006	0.020	0.030	0.693	0.778	0.789	1.080	0.841

Table 5 Kinetic parameters for the adsorption of MB and CV onto MSH

	Methylene blue					Crystal violet				
Intraparticle diffusion model parameters										
$Q_{e\,cal}$ (mg g^{-1})	2.331	4.727	6.512	8.722	10.728	1.285	2.661	3.344	3.814	4.145
K_{1d} (mg g^{-1} min$^{-0.5}$)	0.421	0.85	1.192	1.587	1.946	0.243	0.509	0.646	0.725	0.766
C_1 (mg g^{-1})	0.023	0.074	-0.019	0.03	0.067	-0.049	-0.126	-0.193	-0.156	-0.052
R^2	0.998	0.998	0.999	0.999	0.999	0.998	0.998	0.999	0.999	0.999
%SSE	0.127	0.25	0.035	0.057	0.056	0.153	0.141	0.344	0.009	0.056
RMSE	0.01	0.028	0.015	0.025	0.031	0.007	0.013	0.026	0.005	0.012
HYBRD	0.446	0.625	0.233	0.299	0.296	0.489	0.470	0.733	0.120	0.295
$Q_{e\,cal}$ (mg g^{-1})	2.509	4.815	7.278	9.728	12.13	1.890	3.841	4.933	4.874	5.154
K_{2d} (mg g^{-1} min$^{-0.5}$)	0.02	0.025	0.061	0.083	0.108	0.094	0.183	0.235	0.170	0.189
C_2 (mg g^{-1})	2.207	4.428	6.326	8.447	10.461	0.857	1.836	2.361	3.014	3.087
R^2	0.999	0.999	0.999	0.999	0.999	0.998	0.998	0.998	0.998	0.999
%SSE	0.032	0.005	0.037	0.05	0.064	0.163	0.156	0.156	0.129	0.083
RMSE	0.006	0.004	0.017	0.027	0.037	0.009	0.018	0.023	0.021	0.018
HYBRD	0.224	0.09	0.24	0.279	0.317	0.505	0.493	0.493	0.449	0.361

the desirable ratio is 4, and the ratio of 16.12 and 22.94 obtained for CV and MB removal, respectively, indicates an adequate signal. The models obtained therefore can be used to navigate the design space. Considering all the significant terms, the fitted equations were obtained through regression analysis as shown below.
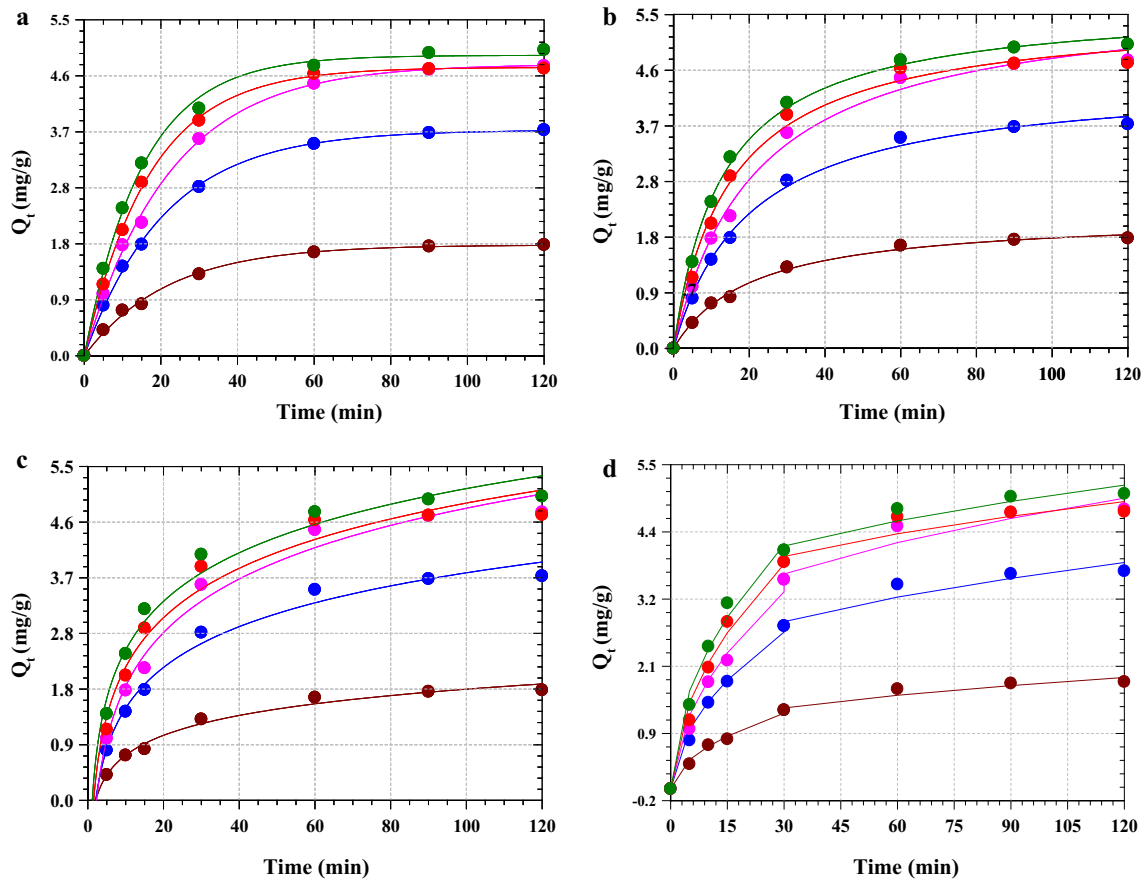
Fig. 10 Kinetics models fits of MB onto MSH: **a** pseudo-first order, **b** pseudo-second order, **c** Elovich and **d** intraparticle diffusion
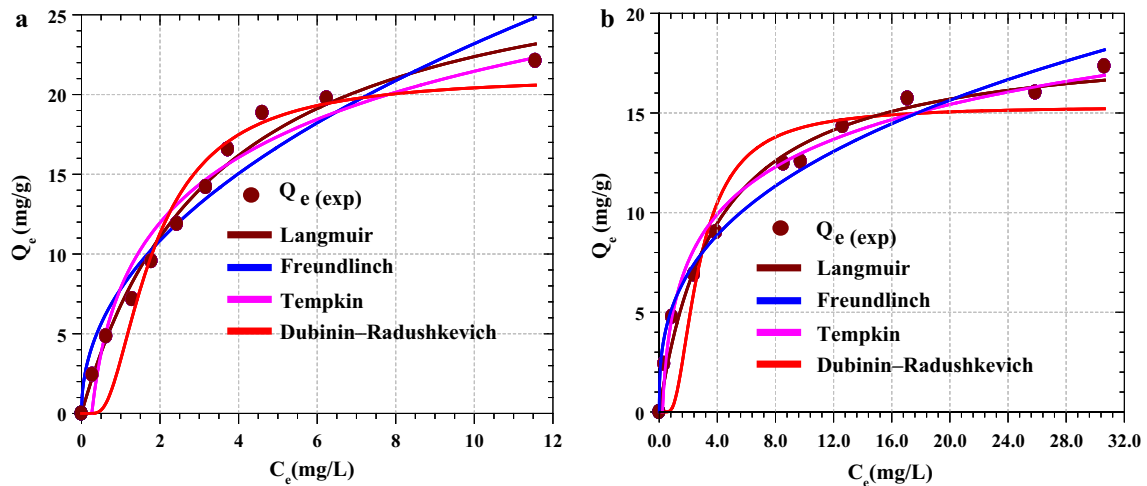

Fig. 11 Adsorption isotherms fits of MB and CV onto MSH

Table 6 Adsorption isotherms parameters for MB and CV onto MSH

Isotherms	Parameters	Values	
		MB	CV
Langmuir	Q_{max} (mg g^{-1})	30.04	18.78
	b (L mg^{-1})	0.292	0.255
	R_L	0.086	0.097
	R^2	0.997	0.997
Freundlich	K_F (g mg^{-1} min$^{-1/n}$)	7.820	5.460
	$1/n$	0.472	0.351
	R^2	0.985	0.995
Tempkin	b_T	427.358	736.684
	a_T (dm^3 mg^{-1})	3.804	4.544
	R^2	0.990	0.997
Dubinin–Radushkevich	Q_s (mg g^{-1})	21.130	15.329
	$\beta \times 10^7$ (mol J^{-1})^2	5.99	1.20
	E (kJ mol^{-1})	0.914	0.646
	R^2	0.984	0.990

Table 7 Comparison of adsorption capacities of different adsorbents for MB and CV

Adsorbents	Q_o (mg g^{-1})	References
Methylene blue		
White pine	38.0	Salazar-Rabago et al. (2010)
Phosphoric acid-treated sago wastes	36.82	Amode et al. (2016)
Bush cane bark	23.49	Enenebeaku et al. (2017)
Banana peel	20.8	Annadurai et al. (2002)
Cereal chaff	20.3	Han et al. (2010)
Spent coffee	18.78	Franca et al. (2009)
MSSH	30.04	This study
Crystal violet		
Bottom ash	12.1	Nidheesh et al. (2012)
Activated carbon	19.8	Malarvizhi and Ho (2010)
Wood apple	19.8	Jain and Jayaram (2010)
Sugarcane dust	3.8	Ho et al. (2005)
Citrullus lanatus rind	11.9	Bharathi and Ramesh (2013)
Jute fibre carbon	27.99	Porkodi and Kumar (2007)
Neem sawdust	4.02	Khattri and Singh (2004)
MSH	18.78	This study

$$\%CV\ Removal = 52.552 + 2.453x_1 + 0.954x_2 + 32.524x_3 - 0.550x_4 + 0.016x_1^2 + 0.001x_2^2$$
$$+ 4.180x_3^2 + 0.009x_4^2 - 0.075x_1x_2 - 2.050x_1x_3 + 0.038x_1x_4$$
$$- 0.449x_2x_3 - 0.005x_2x_4 + 0.076x_3x_4$$

$$\%MB\ Removal = 163.36192 + 1.65057x_1 - 3.30524x_2 + 5.68528\,x_3 - 0.78171x_4$$
$$- 0.16527\,x_1^2 + 0.022432\,x_2^2 - 1.31300\,x_3^2 + 0.010295\,x_4^2 + 0.055822x_1x_2 - 2.50734x_1x_3$$
$$- 0.010788x_1x_4 + 0.49438x_2x_3 + 0.012146x_2x_4 - 0.13722x_3x_4$$

Table 8 Box–Behnken matrix for CV and MB removal by MSH

pH	Temp (°C)	Dosage (mg)	Conc (mg L^{-1})	% Removal of CV			% Removal of MB		
				Actual value	Predicted value	Residue	Actual value	Predicted value	Residue
6.5	40	0.5	30	84.92	84.20	0.72	85.36	85.88	− 0.52
2	40	0.5	50	88.32	87.18	1.14	90.91	90.64	0.27
6.5	30	0.5	10	84.92	84.21	0.71	94.91	96.35	− 1.44
6.5	50	1	30	86.91	88.23	− 1.32	86.91	86.87	0.04
6.5	40	0.5	30	85.76	84.20	1.56	85.36	85.88	− 0.52
6.5	40	1	10	91.66	90.66	1.00	91.13	89.34	1.79
6.5	50	0.1	30	84.93	84.97	− 0.04	78.43	78.65	− 0.22
11	40	1	30	83.92	83.67	0.25	78.30	78.72	− 0.42
11	50	0.5	30	82.92	81.38	1.54	82.70	82.58	0.12
11	30	0.5	30	85.20	85.53	− 0.33	89.19	88.21	0.98
2	40	0.5	10	90.91	91.36	− 0.45	80.92	81.41	− 0.49
2	40	1	30	95.23	95.15	0.08	87.71	89.23	− 1.52
6.5	40	0.5	30	81.92	84.20	− 2.28	86.91	85.88	1.03
11	40	0.5	50	91.91	91.72	0.19	89.91	89.94	− 0.03
2	30	0.5	30	79.91	81.00	− 1.09	93.91	91.99	1.92
6.5	40	1	50	95.12	94.79	0.33	93.91	93.54	0.37
2	40	0.1	30	79.09	79.54	− 0.45	73.93	75.17	− 1.24
6.5	40	0.1	50	85.47	86.11	− 0.64	92.91	92.84	0.07
11	40	0.5	10	80.92	82.32	− 1.40	83.80	84.59	− 0.79
6.5	40	0.1	10	84.92	84.72	0.20	84.92	83.07	1.85
6.5	50	0.5	50	88.56	89.45	− 0.89	92.91	92.99	− 0.08
11	40	0.1	30	84.43	84.67	− 0.24	85.96	85.82	0.14
6.5	30	1	30	89.74	90.08	− 0.34	92.00	92.26	− 0.26
6.5	50	0.5	10	88.91	88.97	− 0.06	79.92	80.84	− 0.92
2	50	0.5	30	91.19	90.42	0.77	77.37	76.31	1.06
6.5	30	0.1	30	79.92	78.74	1.18	92.91	93.51	− 0.60
6.5	30	0.5	50	88.81	88.94	− 0.13	98.18	98.78	− 0.60

The response surface plots shown in Figs. 12 and 13a–f depict the effect of interactions of the factors on the on removal efficiency of CV and MB by the adsorbent. The maximum CV removal efficiency of 90.73% was observed within the range of pH 2 and 11 at 50 °C, lowering temperature below which the removal efficiency reduces (Fig. 12a). The combined effect of pH and adsorbent dosage (Fig. 12b) showed that the simultaneous increase in both factors led to an increase in removal efficiency from 78.9 to 95.2%. The effects pH and initial dye concentration shown in Fig. 12c indicate that increase in pH with dye concentration raised the efficiency by 10%. Removal efficiency decreases from 90.8 to 78.31% as the adsorbent dosage decreases with temperature initially at 50 °C (Fig. 12d). The combined effect of concentration and temperature (Fig. 12e) showed an initial decrease in

efficiency as the concentration increases between 10 and 30 mg dm^{-3}, and further increase in concentration with temperature raised the efficiency to 89.6% from around 82%. Simultaneous increases in the initial dye concentration with adsorbent dosage increase the removal efficiency from 81.6 to 94.8% (Fig. 12f). Similarly, the surface plot of combined effects of the factors is shown in Fig. 13a–f, and the figures depicted similar increase in removal efficiency of MB by the adsorbent. Compared with other combinations, the maximum removal efficiency of 98.7% was noted when concentration and temperature were simultaneously increased. The experimental data were analysed to optimize the removal of CV and MB by selection of goal of each parameter. Targeting the maximum removal efficiency is of with higher importance, hence all parameters were chosen in range within the goal. At

Table 9 Analysis of variance (ANOVA) for the removal of the dyes

Source	Crystal violet					Methylene blue					
	Sum of squares	DF	Mean square	F-value	Prob $> F$	Sum of squares	DF	Mean square	F-value	Prob $> F$	Remark
Model	485.56	14	34.68	18.59	< 0.0001	975.21	14	69.66	36.54	< 0.0001	Significant
$x_{1\text{-pH}}$	22.04	1	22.04	11.82	0.0049	1.29	1	1.29	0.68	0.4270	
$x_{2\text{-Temp}}$	17.43	1	17.43	9.34	0.0100	323.47	1	323.47	169.66	< 0.0001	
$x_{3\text{-Dosage}}$	144.15	1	144.15	77.26	< 0.0001	36.77	1	36.77	19.29	0.0009	
$x_{4\text{-Conc}}$	21.59	1	21.59	11.57	0.0053	152.65	1	152.65	80.07	< 0.0001	
x_1^2	0.54	1	0.54	0.29	0.6007	59.76	1	59.76	31.35	0.0001	
x_2^2	0.02	1	0.02	0.01	0.9154	26.85	1	26.85	14.08	0.0028	
x_3^2	3.71	1	3.71	1.99	0.1841	1.27	1	1.27	0.67	0.4299	
x_4^2	70.20	1	70.20	37.62	< 0.0001	90.42	1	90.42	47.43	< 0.0001	
$x_1 x_2$	45.97	1	45.97	24.64	0.0003	25.25	1	25.25	13.24	0.0034	
$x_1 x_3$	69.52	1	69.52	37.27	< 0.0001	112.90	1	112.90	59.22	< 0.0001	
$x_1 x_4$	46.10	1	46.10	24.71	0.0003	3.76	1	3.76	1.97	0.1854	
$x_2 x_3$	16.47	1	16.47	8.83	0.0117	22.58	1	22.58	11.85	0.0049	
$x_2 x_4$	4.49	1	4.49	2.41	0.1466	23.62	1	23.62	12.39	0.0042	
$x_3 x_4$	1.90	1	1.90	1.02	0.3334	7.81	1	7.81	4.09	0.0659	
Residual	22.39	12	1.87			22.88	12	1.91			
Lack of fit	14.24	10	1.42	0.35	0.8960	21.28	10	2.13	2.66	0.3043	Not significant
Pure error	8.15	2	4.08			1.60	2	0.80			
Cor total	507.95	26				998.08	26				

Table 10 Correlation coefficient of the ANOVA

	CV	MB
R-squared	0.956	0.977
Adj R-squared	0.905	0.950
Pred R-squared	0.799	0.872
Adeq precision	16.119	22.944
C.V.	1.578	1.586

chosen criterions, the optimum conditions obtained with desirability of 1 were as follows: pH 10.49, temperature 30.84 °C, adsorbent dosage 0.95 g/25 cm³ and initial dye concentration of 47.59 mg L⁻¹ for the removal of 86.1% CV, whereas 99.01% MB was removed at pH 6.14, temperature 30.18 °C, adsorbent dosage 0.21 g/25 cm³ and initial dye concentration of 48.92 mg dm⁻³. The predicted optimized condition was chosen as a basis for validating the model experimentally. The experiments were carried out in triplicates and the average maximum removal obtained as 83.72 and 97.35% for CV and MB, respectively, and hence, the experimental and predicted responses show

close proximity. Hence, it could be concluded that experimental procedure follows the predicted optimized condition by selected quadratic model.

Adsorption thermodynamic study

The van't Hoff plot for the removal of CV and MB by MSH is shown in Fig. 14, while the thermodynamics parameters are presented in Table 10.

The thermodynamic parameters (Table 11) obtained for the dyes revealed that the enthalpies of the adsorption, $\Delta H°$, are positive, connoting increase in adsorption efficiency with increase in process temperature while the positive values of entropies, $\Delta S°$, indicated that there was an affinity between the dyes molecules and adsorbents surfaces and that the degree of dispersion of the process increased with increase in temperature. The spontaneity of the adsorption of CR by the adsorbents was revealed by the negative Gibbs free energy (ΔG) values obtained at various temperatures suggesting favourable adsorption of CR by the adsorbents at higher temperature (Adeogun et al. 2018).
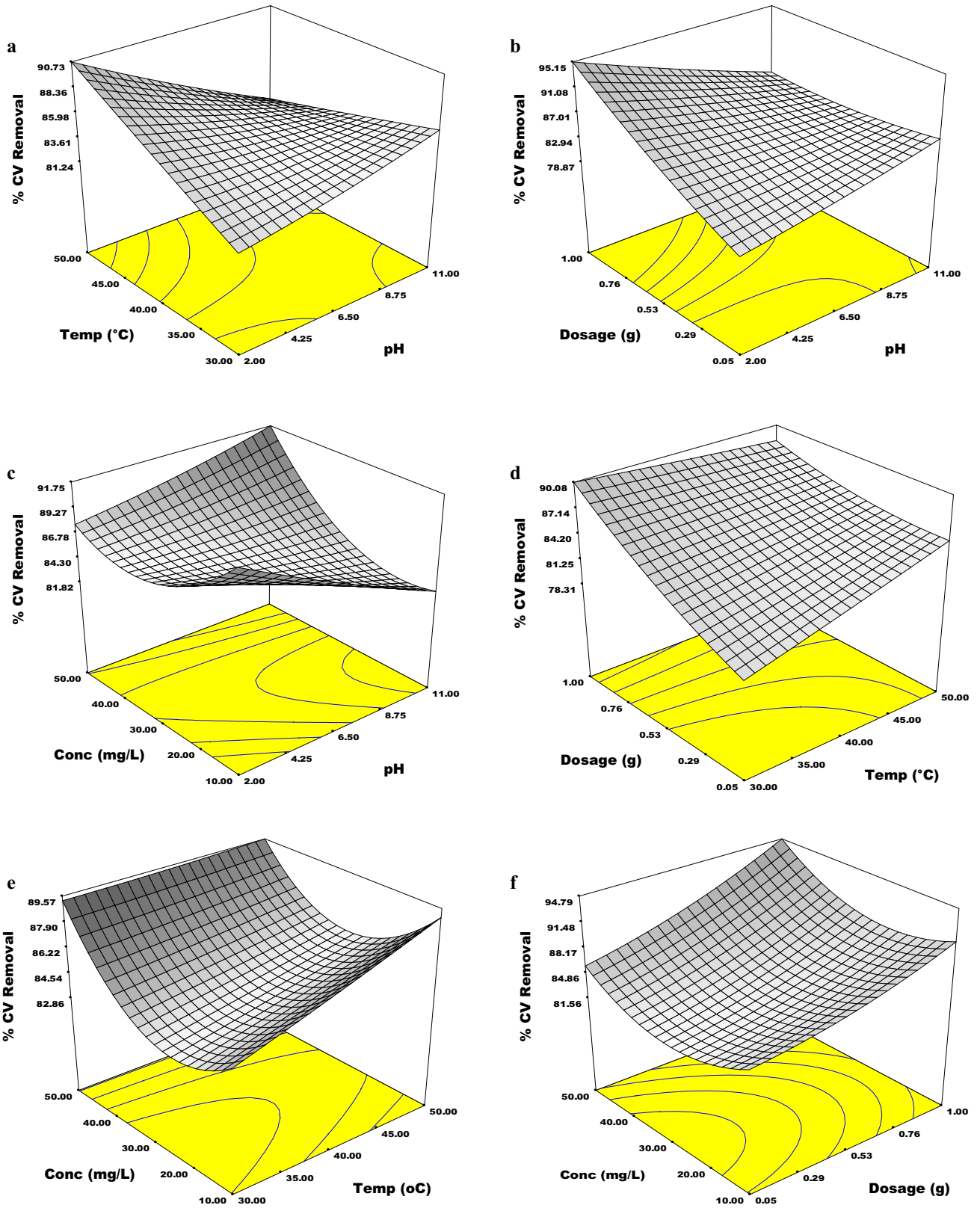
Fig. 12 Response surface plot for the removal efficiency of CV onto MSH
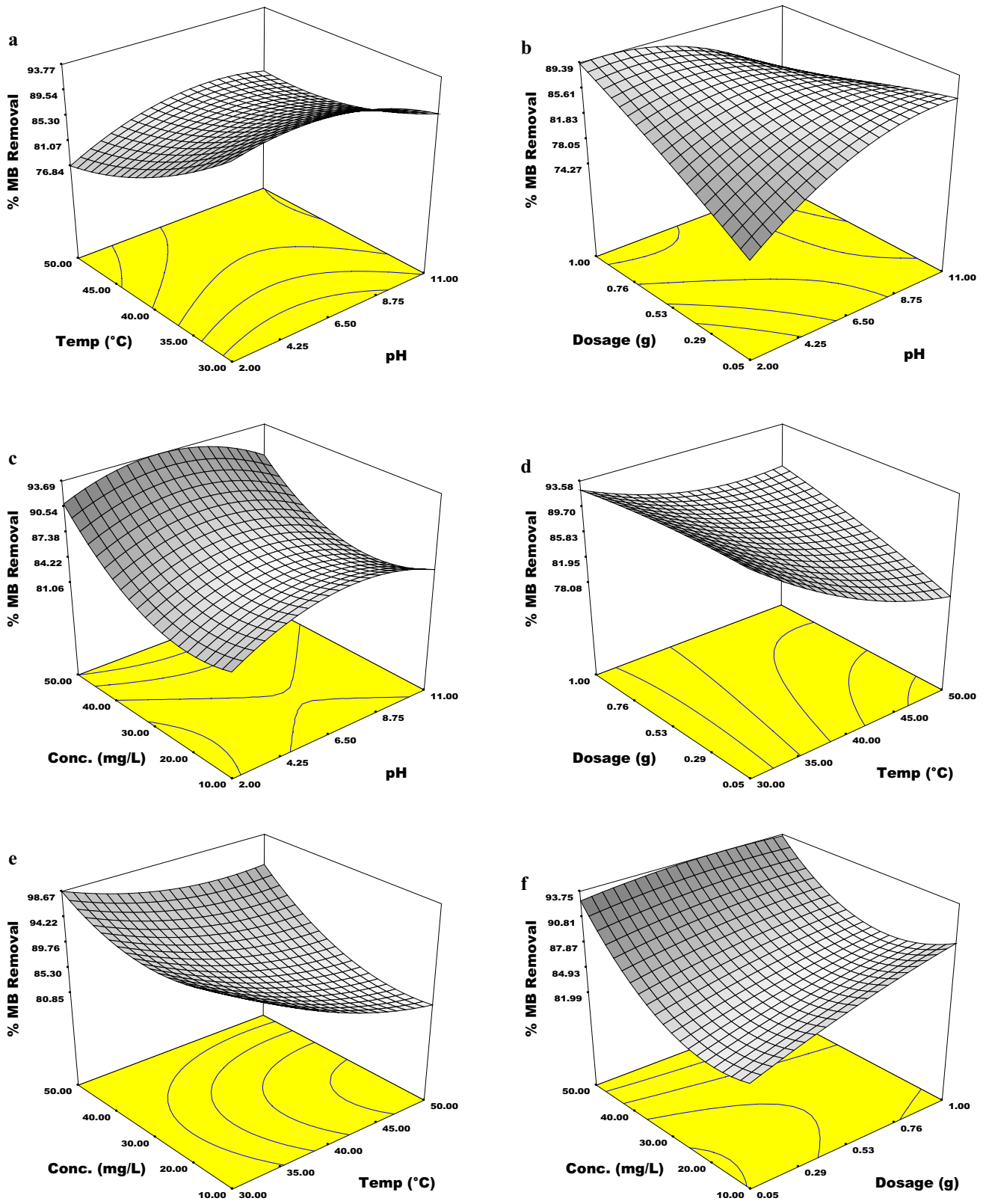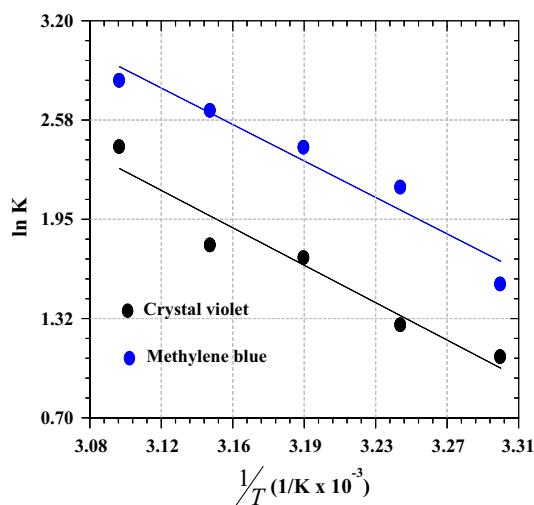
Fig. 13 Response surface plot for the removal efficiency of MB onto MSH

Table 11 Thermodynamic parameters for adsorption of CV and MB by MSH

Temp (K)	CV					MB				
	ln K_d	ΔG (kJ mol^{-1})	ΔH (kJ mol^{-1})	ΔS (J mol^{-1} K^{-1})	R^2	ln K_d	ΔG (kJ mol^{-1})	ΔH (kJ mol^{-1})	ΔS (J mol^{-1} K^{-1})	R^2
308.15	1.282	−3.431	56.943	195.379	0.921	2.149	−5.142	37.247	138.760	0.997
313.15	1.705	−4.317				2.400	−6.034			
318.15	1.785	−5.204				2.632	−6.926			
323.15	2.404	−6.091				2.821	−7.818			

Fig. 14 van't Hoff fit for adsorption of CV and MB by MSH

Conclusion

Magnetic tuned biosorbent (MSH) from sorghum husk biomass was successfully prepared and used as adsorbent for the removal of CV and MB from aqueous solution. The batch adsorption processes for the dyes removal are contact time, initial pollutant concentration, solution pH, adsorbent dosage and temperature dependent. The kinetics of adsorption of the dyes were best explained with pseudo-first-order kinetics, while adsorption Langmuir isotherm model fitted the equilibrium data with monolayer capacity of 30.13 and 15.33 mg g^{-1} for MB and CV, respectively. The statistical analysis showed that the predicted models are suitable for the prediction of the adsorption process with $R^2 > 0.9$ for the two dyes. The thermodynamic parameters proved that the adsorption process is feasible, spontaneous, endothermic and random in nature. The study indicates that magnetic supported sorghum husk is a promising adsorbent for the adsorption of methylene blue and crystal violet dyes from aqueous solution.

Compliance with ethical standards

Conflict of interest The authors hereby declare that there is no conflict of interests regarding the publication of this article.

Open Access This article is distributed under the terms of the Creative Commons Attribution 4.0 International License (http://creativecommons.org/licenses/by/4.0/), which permits unrestricted use, distribution, and reproduction in any medium, provided you give appropriate credit to the original author(s) and the source, provide a link to the Creative Commons license, and indicate if changes were made.

References

Adeogun AI, Idowu MA, Akiode KO, Ahmed SA (2016) Bioremediation of Cu(II) contaminated water by *Saccharum officinarum*: effect of oxalic acid modification on equilibrium, kinetic and thermodynamic parameters. Bioresour Bioprocess 3:7

Adeogun AI, Ofudje EA, Idowu MA, Kareem SO, Vahidhabanu S, Babu BR (2018) Biosorption of Cd^{2+} and Zn^{2+} from aqueous solution using tilapia fish scale (*Oreochromis* sp): kinetics, isothermal and thermodynamic study. Desalination Water Treat 107:182–194

Ahmad R (2009) Studies on adsorption of crystal violet dye from aqueous solution onto coniferous pinus bark powder (CPBP). J Hazard Mater 171:767–773

Ait Ahsaine H, Zbair M, Anfar Z, Naciri Y, El haouti R, El Alem N, Ezahri M (2018) Cationic dyes adsorption onto high surface area 'almond shell' activated carbon: kinetics, equilibrium isotherms and surface statistical modeling. Mater Today Chem 8:121–132

Akinola LK, Umar AM (2015) Adsorption of crystal violet onto adsorbents derived from agricultural wastes: kinetic and equilibrium studies. J Appl Sci Environ Manag 19(2):279–288

Amode JO, Santos JH, Alam ZM, Mirza AH, Mei CC (2016) Adsorption of methylene blue from aqueous solution using untreated and treated (*Metroxylon* spp.) waste adsorbent: equilibrium and kinetics studies. Int J Ind Chem 7(3):333–345

Annadurai G, Juang RS, Lee DJ (2002) Use of cellulose based wastes for adsorption of dyes from aqueous solutions. J Hazard Mater B29:263–274

Bestani B, Benderdouche N, Benstaali B, Belhakem M, Addou A (2008) Methylene blue and iodine adsorption onto an activated desert plant. Biores Technol 99(17):8441–8444

Bharathi KS, Ramesh ST (2013) Removal of dyes using agricultural waste as low-cost adsorbents: a review. Appl Water Sci 3(4):773–790

Cheu SC, Kong H, Song ST, Johari K, Saman N, Yunus MAC, Mat H (2016) Separation of dissolved oil from aqueous solution by sorption onto acetylated lignocellulosic biomass—equilibrium,

kinetics and mechanism studies. J Environ Chem Eng 4(1):864–881

Dhawane SH, Kumar T, Halder G (2016) Biodiesel synthesis from *Hevea brasiliensis* oil employing carbon supported heterogeneous catalyst: optimization by Taguchi method. Renew Energy 89:506–514

Dubinin MM, Radushkevich LV (1947) The equation of the characteristic curve of the activated charcoal. Proc Acad Sci USSR Phys Chem Sect 55:331–337

El-Khaiary MI (2008) Least-squares regression of adsorption equilibrium data: comparing the options. J Hazard Mater 158(1):73–87

Elovich SY, Larionov OG (1962) Theory of adsorption from nonelectrolyte solutions on solid adsorbents. Bull Acad Sci USSR Div Chem Sci 11:198–203

El-Sayed GO (2011) Removal of methylene blue and crystal violet from aqueous solutionsby palm kernel fiber. Desalination 272:225–232

Enenebeaku CK, Okorocha NJ, Enenebeaku UE, Onyeachu BI (2017) Adsorption of methylene blue dye onto bush cane bark powder. Int Lett Chem Phys Astron 76:12–26

Franca AS, Oliveira LS, Ferreira ME (2009) Kinetics and equilibrium studies of methylene blue adsorption by spent coffee grounds. Desalination 249(1):267–272

Freundlich HMF (1906) Over the adsorption in solution. J Phys Chem 57:385–471

Gao W, Zhao S, Wu H, Deligeer W, Asuha S (2016) Direct acid activation of kaolinite and its effects on the adsorption of methylene blue. Appl Clay Sci 126:98–106

Ghosh D, Bhattacharyya KG (2002) Adsorption of methylene blue on kaolinite. Appl Clay Sci 20(6):295–300

Han R, Zhang L, Song C, Zhang M, Zhu H, Zhang L (2010) Characterization of modified wheat straw, kinetic and equilibrium study about copper ion and methylene blue adsorption in batch mode. Carbohydr Polym 79(4):1140–1149

Hanbali M, Holail H, Hammud H (2014) Remediation of lead by pretreated red algae: adsorption isotherm, kinetic, column modeling and simulation studies. Green Chem Lett Rev 7(4):342–358

Ho YS, McKay G (1998) Kinetic models for the sorption of dye from aqueous solution by wood. Process Saf Environ Prot 76(2):183–191

Ho YS, McKay G (1999) Pseudo-second order model for sorption processes. Process Biochem 34(5):451–465

Ho YS, Chiu WT, Wang CC (2005) Regression analysis for the sorption isotherms of basic dyes on sugarcane dust. Bioresour Technol 96(11):1285–1291

Hussein A, Scholz M (2018) Treatment of artificial wastewater containing two azo textile dyes by vertical-flow constructed wetlands. Environ Sci Pollut Res 25(7):6870–6889

Jain S, Jayaram RV (2010) Removal of basic dyes from aqueous solution by low-cost adsorbent: wood apple shell (*Feronia acidissima*). Desalination 250(3):921–927

Kakavandi B, Takdastan A, Jaafarzadeh N, Azizi M, Mirzaei A, Azari A (2016) Application of Fe_3O_4@C catalyzing heterogeneous UV-Fenton system for tetracycline removal with a focus on optimization by a response surface method. J Photochem Photobiol A 314:178–188

Khattri SD, Singh MK (2004) Colour removal from synthetic dye wastewater using a bioadsorbent. Water Air Soil Pollut 120(3–4):283–294

Langmuir I (1916) The constitution and fundamental properties of solids and liquids. Part I. Solids. J Am Chem Soc 38(11):2221–2295

Luo P, Zhao Y, Zhang B, Liu J, Yang Y, Liu J (2010) Study on the adsorption of Neutral Red from aqueous solution onto halloysite nanotubes. Water Res 44(5):1489–1497

Maksin DD, Nastasović AB, Milutinović-Nikolić AD, Suručić LT, Sandić ZP, Hercigonja RV, Onjia AE (2012) Equilibrium and kinetics study on hexavalent chromium adsorption onto diethylene triamine grafted glycidyl methacrylate based copolymers. J Hazard Mater 209:99–110

Malarvizhi R, Ho YS (2010) The influence of pH and the structure of the dye molecules on adsorption isotherm modeling using activated carbon. Desalination 264(1–2):97–101

Nidheesh PV, Gandhimathi R, Ramesh ST, Singh TSA (2012) Adsorption and desorption characteristics of crystal violet in bottom ash column. J Urban Environ Eng 6(1):18–29

Ozdes D, Duran C, Senturk HB, Avan H, Bicer B (2014) Kinetics, thermodynamics, and equilibrium evaluation of adsorptive removal of methylene blue onto natural illitic clay mineral. Desalination Water Treat 52(1–3):208–218

Pathania D, Sharma S, Singh P (2010) Removal of methylene blue by adsorption onto activated carbon developed from Ficus carica bast. Arab J Chem 710:S1445–S1451

Pereira L, Alves M (2012) Dyes—environmental impact and remediation. In: Malik A, Grohmann E (eds) Environmental protection strategies for sustainable development. Springer, Dordrecht, pp 111–162

Porkodi K, Kumar KV (2007) Equilibrium, kinetics and mechanism modeling and simulation of basic and acid dyes sorption onto jute fiber carbon: eosin yellow, malachite green and crystal violet single component systems. J Hazard Mater 143(1–2):311–327

Rathod M, Mody K, Basha S (2014) Efficient removal of phosphate from aqueous solutions by red seaweed, *Kappaphycus alverezii*. J Clean Prod 84:484–493

Raveendra RS, Prashanth PA, Hari Krishna R, Bhagya NP, Nagabhushana BM, Raja Naika H, Lingaraju K, Nagabhushana H, Daruka Prasad B (2014) Synthesis, structural characterization of nano ZnTiO3 ceramic: an effective azo dye adsorbent and antibacterial agent. J Asian Ceram Soc 2(4):357–365

Saeed A, Sharif M, Iqbal M (2010) Application potential of grapefruit peel as dye sorbent: kinetics, equilibrium and mechanism of crystal violet adsorption. J Hazard Mater 179:564–572

Salazar-Rabago JJ, Leyva-Ramos R, Rivera-Utrilla J, Ocampo-Perez R, Cerino-Cordova FJ (2010) Biosorption mechanism of methylene blue from aqueous solution onto white pine (*Pinus durangensis*) sawdust: effect of operating conditions. Sustain Environ Res 27(1):32–40

Schwertmann U, Cornell RM (2008) Iron oxides in the laboratory: preparation and characterization. Wiley

Tempkin MI, Pyzhev V (1940) Kinetics of ammonia synthesis on promoted iron catalyst. Acta Phys Chim USSR 12:327–356

Vassileva P, Detcheva A, Uzunov I, Uzunova S (2013) Removal of metal ions from aqueous solutions using pyrolyzed rice husks: adsorption kinetics and equilibria. Chem Eng Commun 200(12):1578–1599

Weber WJ, Morris JC (1963) Kinetics of adsorption on carbon from solution. J Sanit Eng Div 89:31–59

Wong H-W, Phillips DL, Ma C-Y (2007) Raman spectroscopic study of aminated food proteins. Food Chem 105:784–792